

Figure 1: Maxwellian with ITER-relevant parameters $T = 20\text{keV}$ and $n = 10^{20} \text{ m}^{-3}$ in various coordinate systems. (a) $f_{Car}^{3D}(v_{\parallel}, v_{\perp 1}, v_{\perp 2})$. (b) $f_{Car}^{3D}(v_{\parallel}, v_{\perp})$. (c) $f_{Car}^{2D}(v_{\parallel}, v_{\perp})$. (d) $f_{Ep}^{2D}(E)$. The units in (a) and (b) are s^3/m^6 , in (c) $10^6 \text{ s}^2/\text{m}^5$, and in (d) $10^{14}/(\text{eVm}^3)$. The isotropy of the Maxwellian is reflected in the concentric isolines in (a) and (b) and in the dependence of the function on the pitch in (d). However, in (c), the Jacobian v_{\perp} conceals the isotropy as f_{Car}^{2D} approaches zero close to the v_{\parallel} axis, where $v_{\perp} \rightarrow 0$. Likewise, $f_{Ep}^{2D}(E)$ approaches zero for $E \rightarrow 0$.

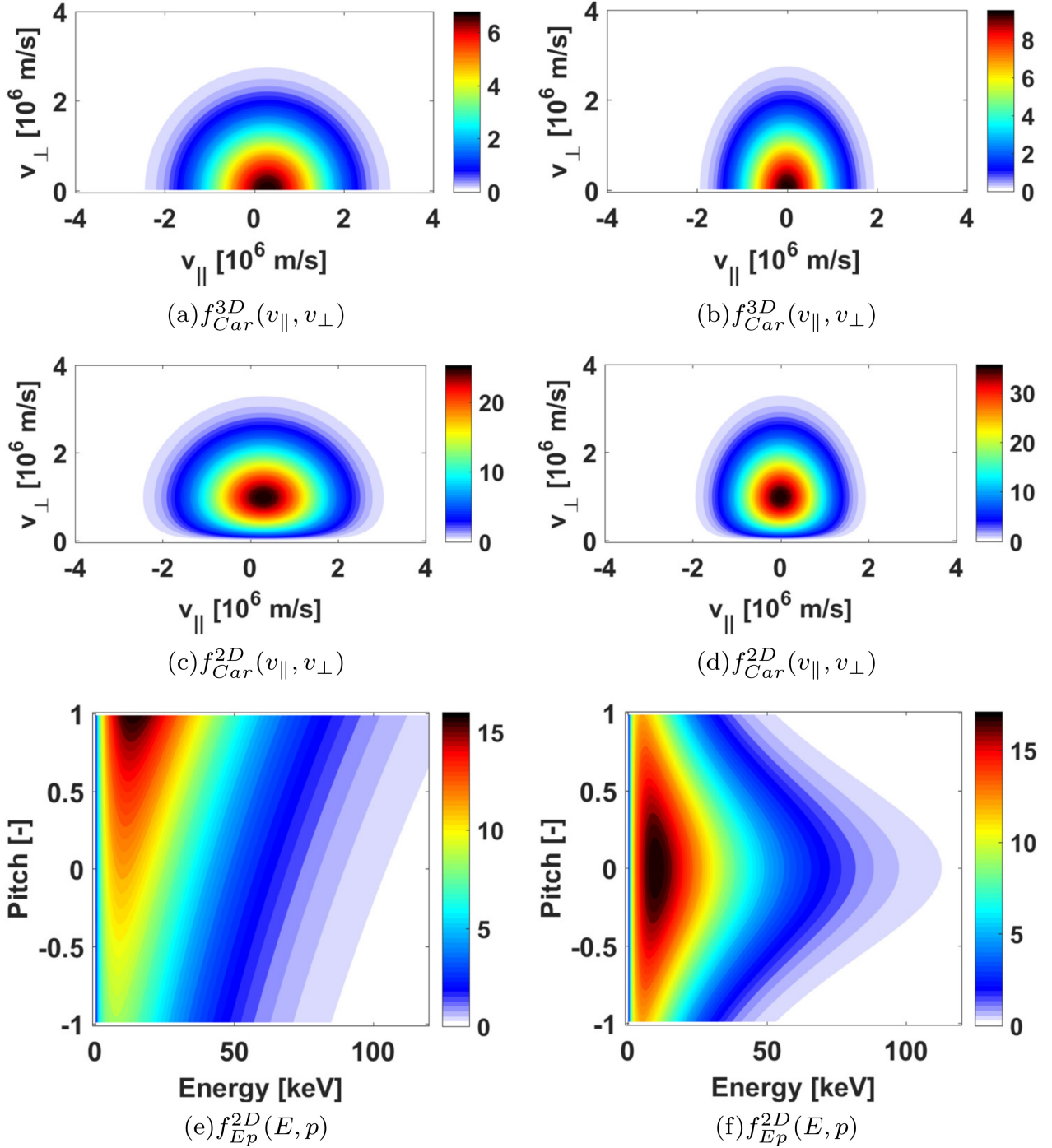


Figure 2: Drifting Maxwellians and biMaxwellians in three coordinate systems. The baseline parameters are $T = 20\text{keV}$ and $n = 10^{20}\text{m}^{-3}$ as in Fig. 1. However, in (a), (c), and (e), we set $v_d = 3 \times 10^5\text{m/s}$, and in (b), (d), and (f), we set $T_k = 10\text{keV}$ and $T_{\perp} = 20\text{keV}$. Drift is reflected in the translation in the v_{\parallel} direction for $(v_{\parallel}, v_{\perp})$ coordinates and in the bias towards positive p in (E, p) coordinates. Temperature anisotropy is reflected in the departure from the circular shape in (b) and from straight lines in (f).

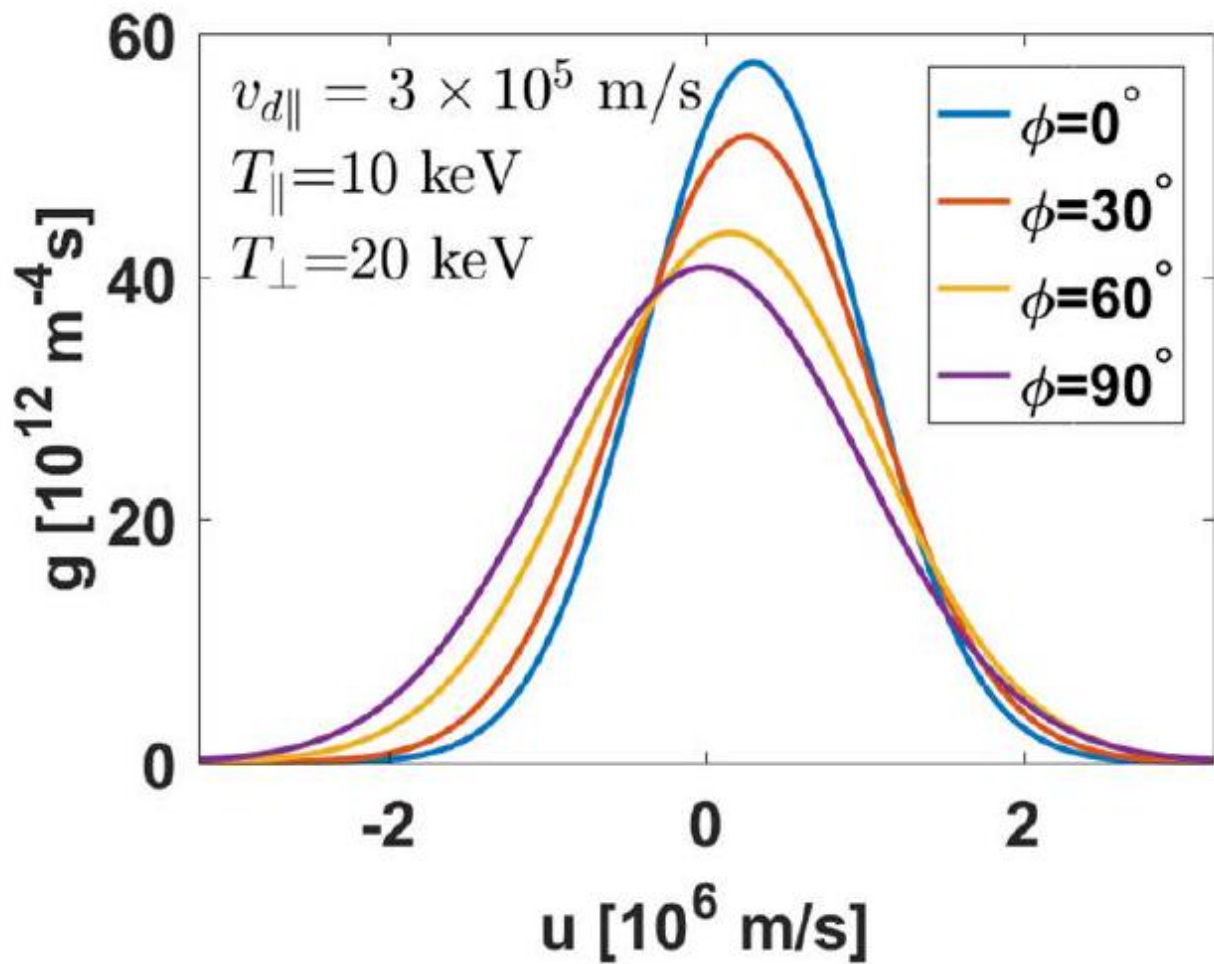
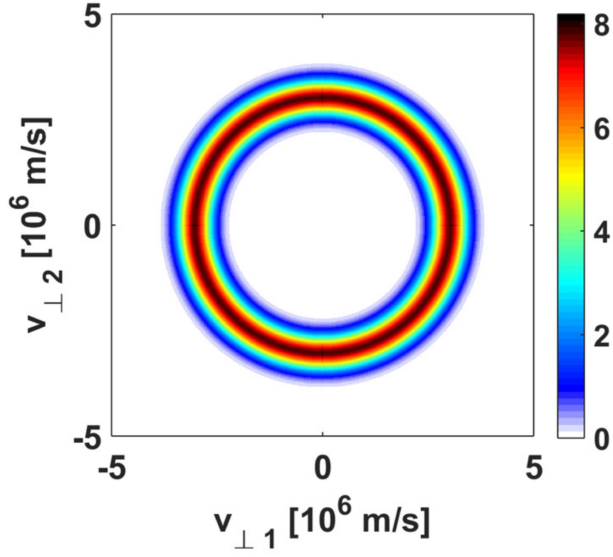
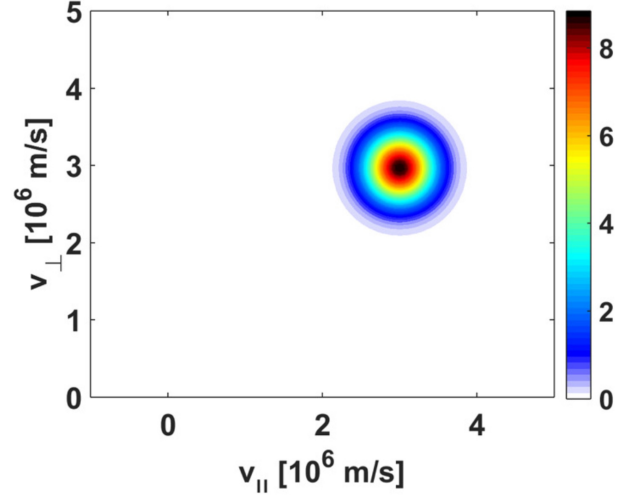


Figure 3: 1D projections at various projection angles of a bi-Maxwellian with drift parallel to the magnetic field. The more parallel the view, the narrower the function due to the smaller temperature and the larger the shift in u due to the parallel drift velocity.



(a) $f_{Car}^{3D}(v_{\parallel}, v_{\perp 1}, v_{\perp 2})$



(b) $f_{Car}^{3D}(v_{\parallel}, v_{\perp})$

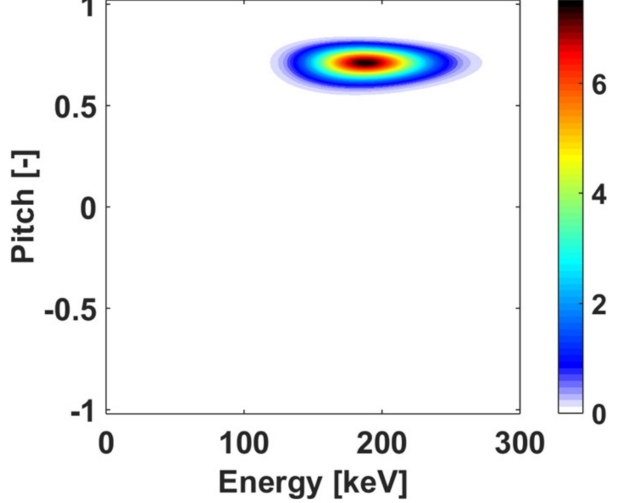
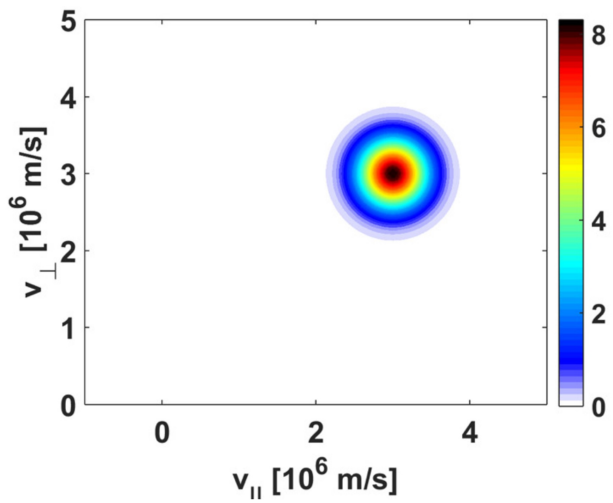


Figure 4: Ring distribution (a.u.) in various coordinate systems. The ring distributions in 3D (b) and 2D (c) look similar, but in the 2D distribution, a small bias towards large velocities is introduced by the factor $2\pi v_{\perp} \cdot \ln(E, p)$ -coordinates, the ring distribution looks fairly distorted.

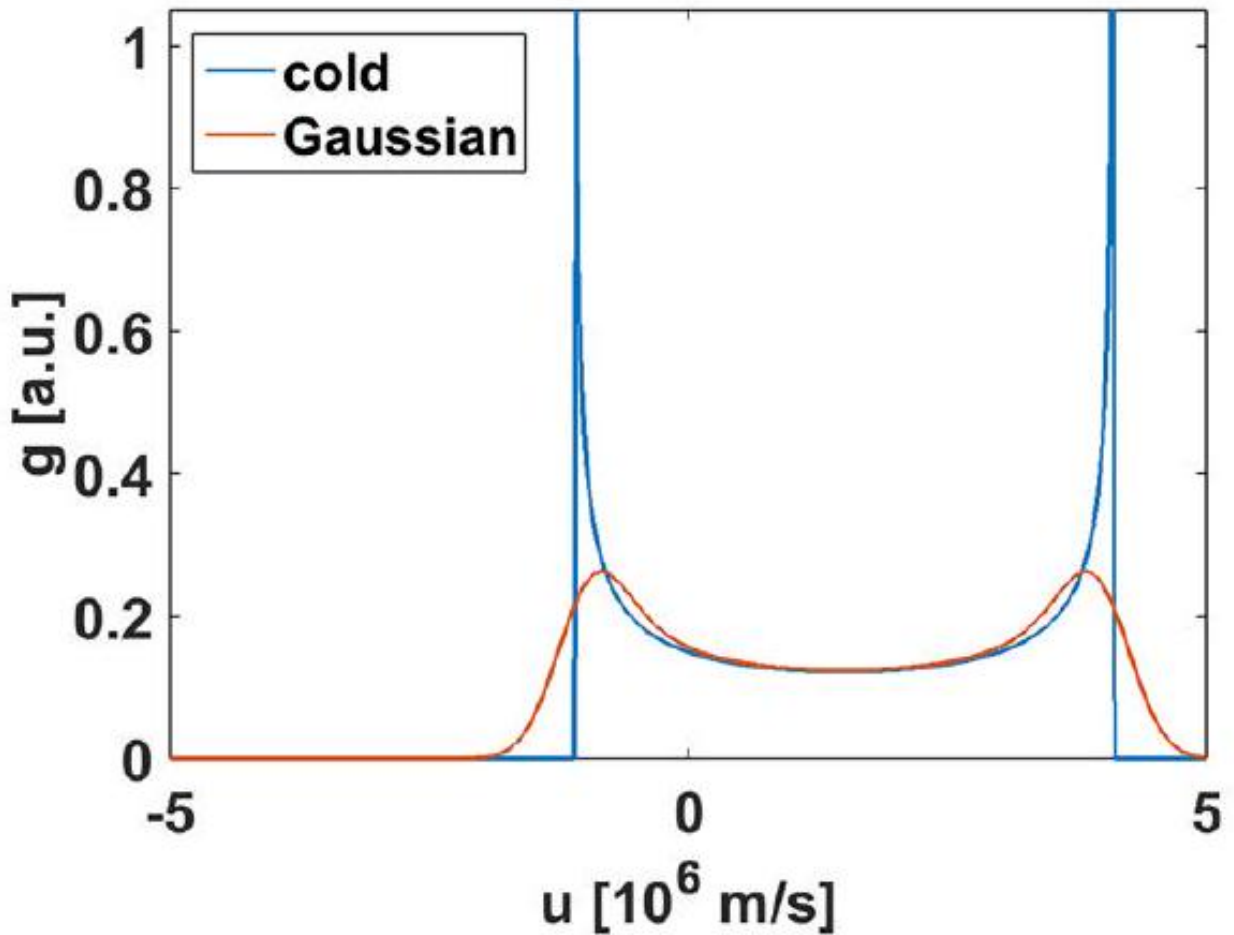


Figure 5: 1D projections of a cold ring distribution and a warm ring distribution where the δ -function is replaced by a Gaussian function in 2D $(v_{\parallel}, v_{\perp})$ -space. The center of the function is at $v_{\parallel 0} \cos \phi$, and the width is $v_{\perp 0} \sin \phi$.

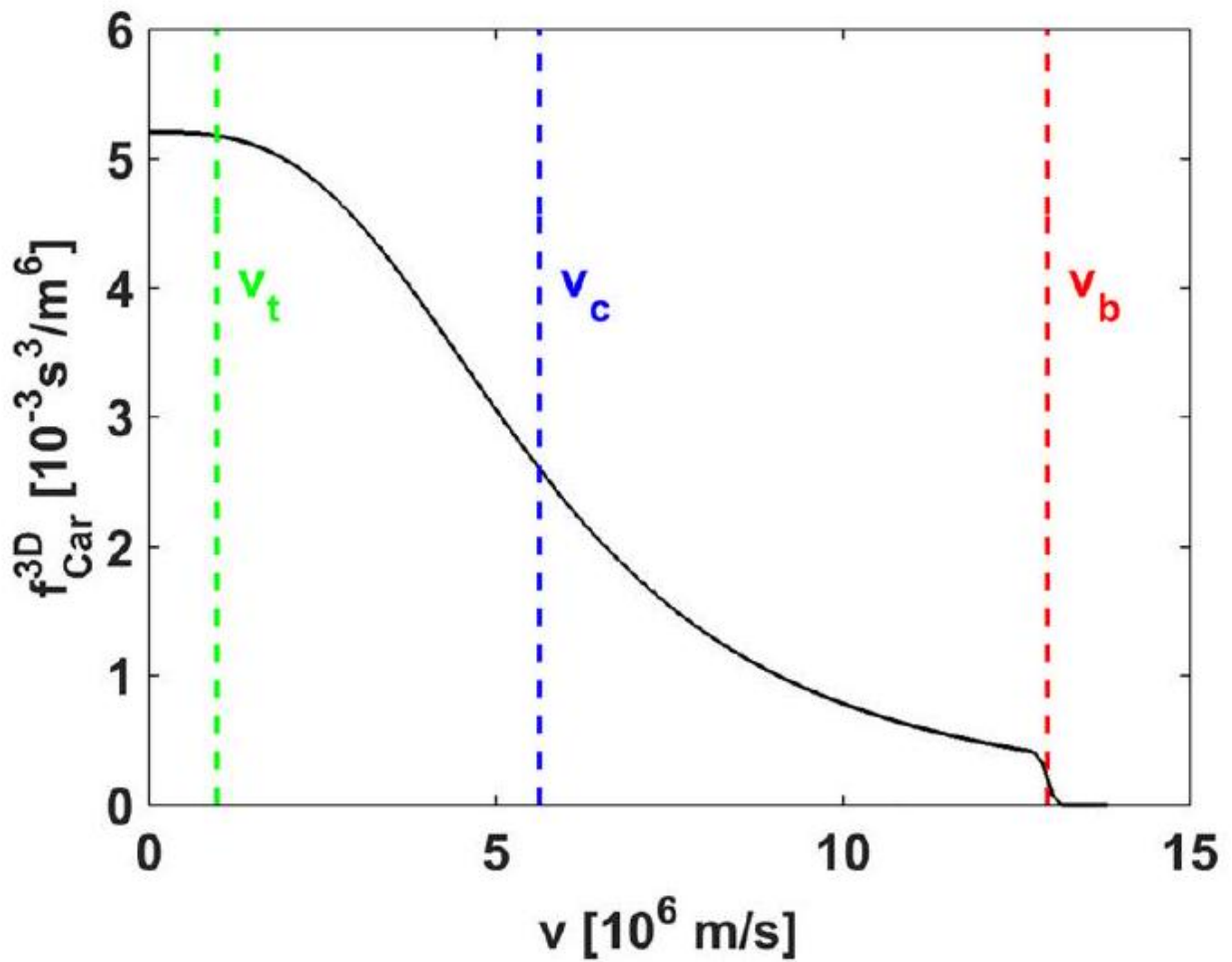


Figure 6: Slowing-down distribution function $f_{Car}^{3D}(v)$ for α -particles in ITER. The birth speed, the crossover speed, and the thermal speed are marked.

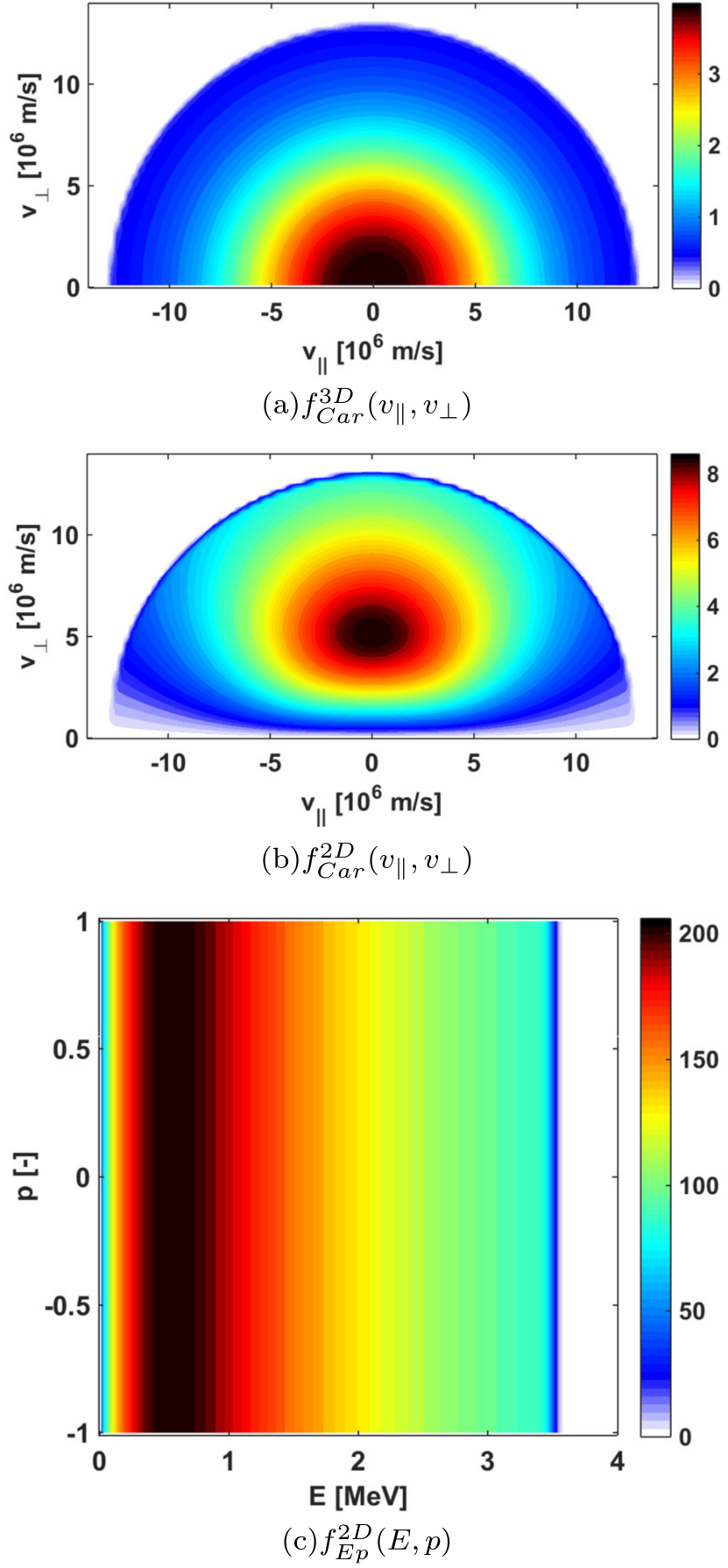


Figure 7: α -particle slowing-down velocity distribution function with ITER-relevant parameters in various coordinate systems. No ions above the birth energies are found.

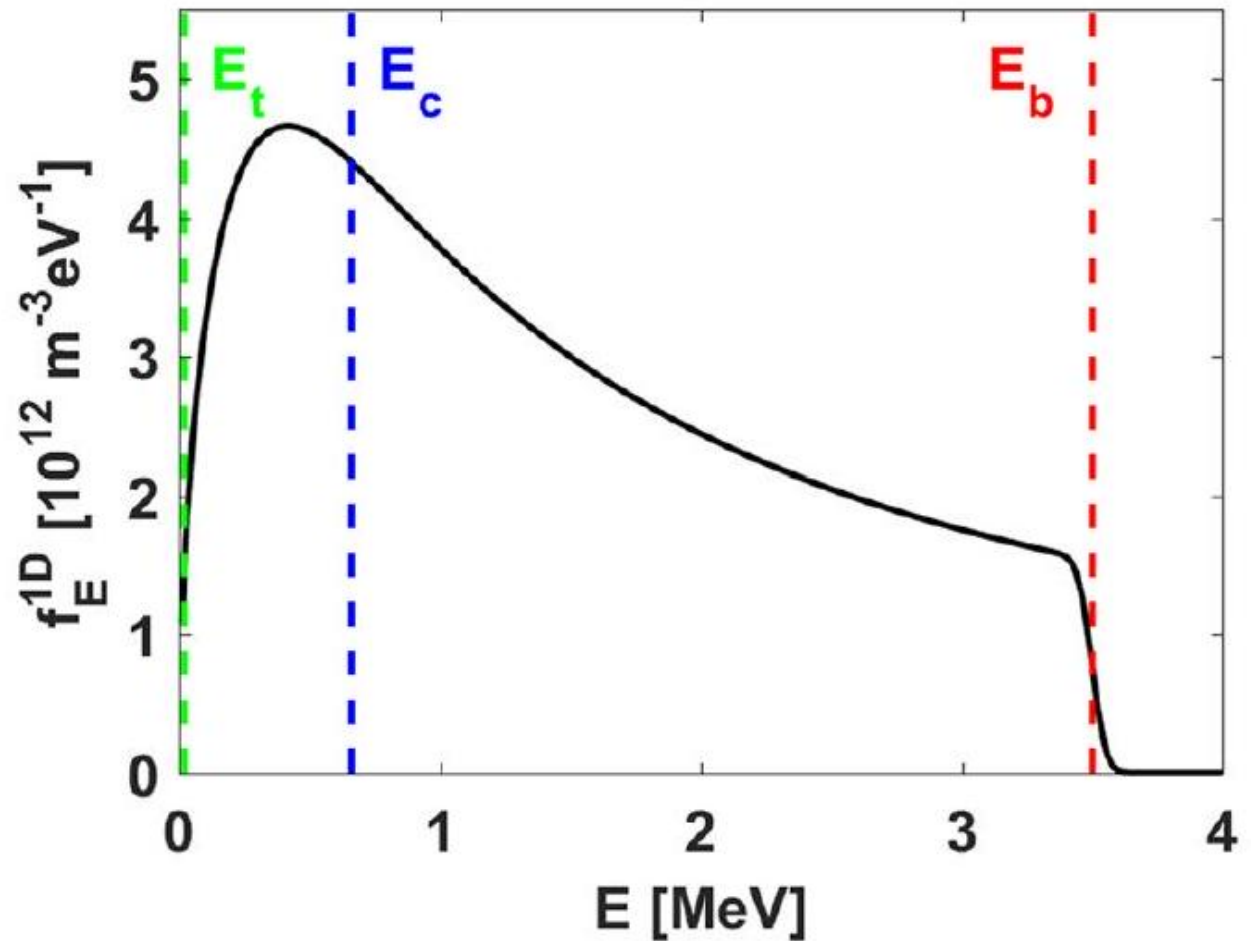


Figure 8: α -particle slowing-down energy distribution function as expected in ITER. The energy distribution function is more flat as compared to Fig. 6.

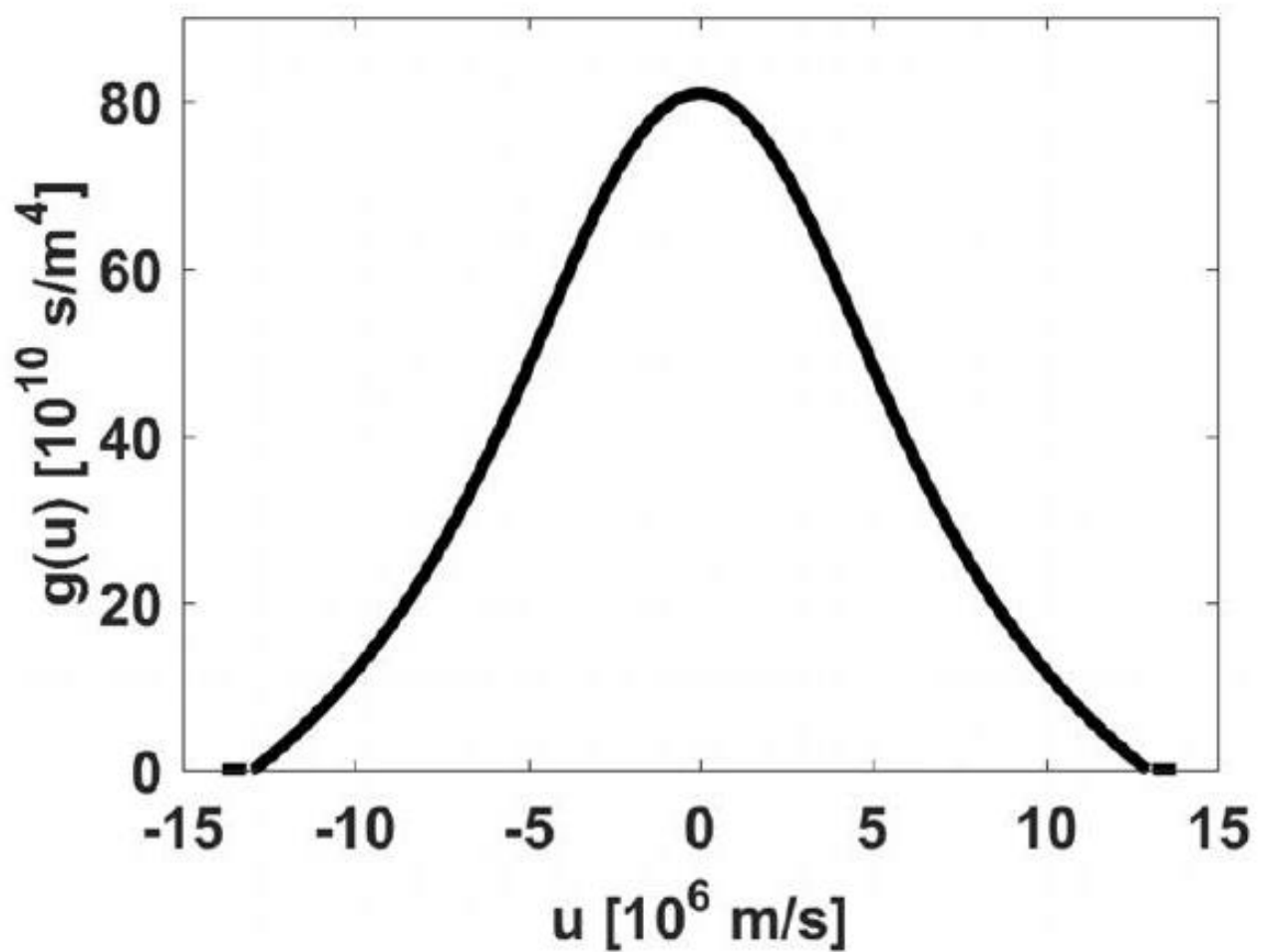


Figure 9: 1D projection of the isotropic α -particle slowing-down distribution function $g(u)$ for any projection angle ϕ as expected for ITER.

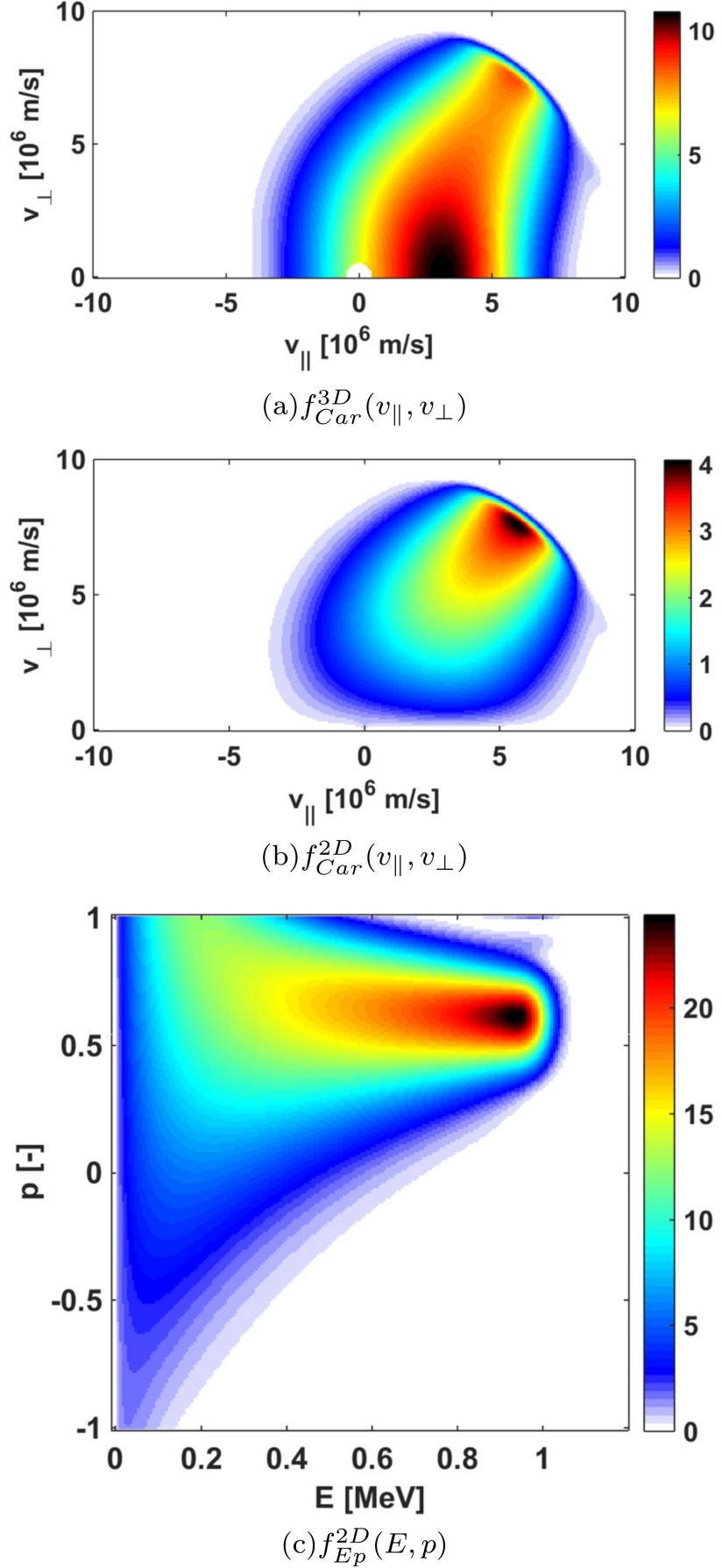


Figure 10: NBI distribution function in various coordinate systems showing the slowing down and pitch angle scattering of a particle source at an energy of 1 MeV at a pitch of 0.6. The pitch coordinate is essential for the use of Legendre polynomials so that the expressions are by far simplest when the pitch is used as a coordinate. Therefore, we do not give explicit expressions in the other coordinate systems and transform the function numerically in Fig. 10.

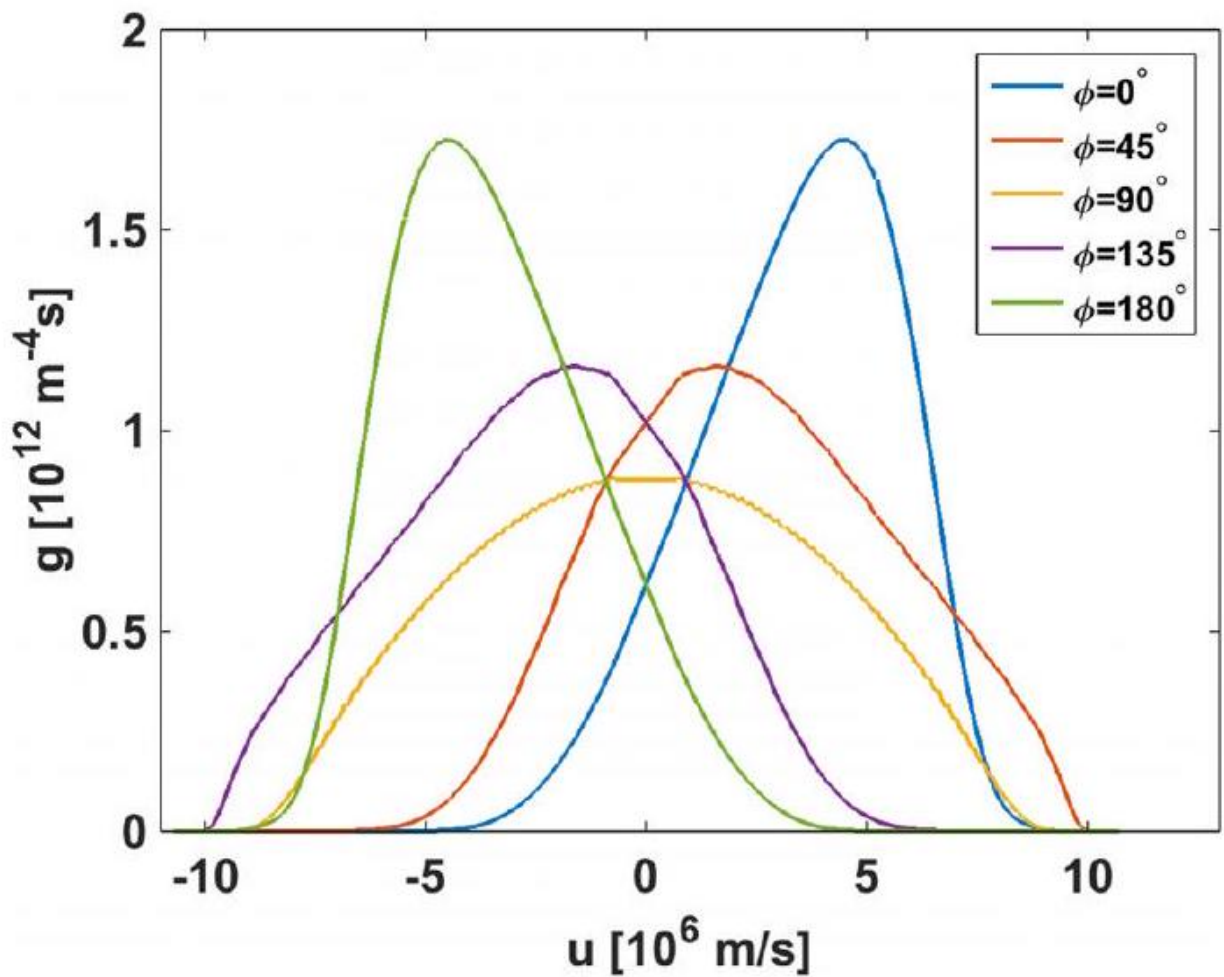


Figure 11: 1D projections of the NBI distribution function from Fig. 10 for various projection angles ϕ .